Coordinated pitch and torque control of wind farms for power tracking

Carl R. Shapiro,[1] Johan Meyers,[2] Charles Meneveau,[1] and Dennice F. Gayme[1]

Abstract— **Improved integration of wind farms into frequency regulation services is vital for increasing renewable energy production while ensuring power system stability. This work generalizes a recently proposed model-based receding horizon wind farm controller for secondary frequency regulation to arbitrary wind farm layouts and augments the controller to enable power modulation through storage of kinetic energy in the rotor. The new design explicitly includes actuation of blade pitch and generator torque, which facilitates implementation in existing farms as it takes advantage of current wind turbine control loops. This generalized control design improves control authority by individually controlling each turbine and using kinetic energy stored in the rotor in a coordinated manner to achieve farm level control goals. Numerical results demonstrate the effectiveness of this approach; in particular, the controller achieves accurate power tracking and reduces loss of revenue in the bulk power market by requiring less setpoint reduction (derate) than the power level control range.**

I. INTRODUCTION

Control designs that allow wind farms to participate in a variety of grid services are vital for increasing wind power penetration in the electric power grid. As growing wind power generation displaces conventional power plants that typically provide frequency regulation services, regulators are considering requiring wind plants to provide these services [1], [2]. Use of wind farms to provide secondary frequency regulation, a service where participating generators follow a power reference signal sent by the grid operator, is a particular area of growing interest [2], [3], [4].

Power plants participating in secondary frequency regulation typically provide power in both the bulk power market and the regulation market. The bulk power is supplied at some fixed level and the regulation service entails following a regulation signal sent by the grid operator. While current wind turbine controllers operate at the maximum power point, participation in the secondary frequency regulation market — which includes increased power demand over the bulk power setpoint — requires a wind farm to reduce the amount of power it provides to the bulk power market [2], [5], [6], [7], [8], [9]. New control designs should therefore enable wind farms to provide power tracking [2], [10] while reducing lost revenue in bulk power markets [5], [6].

*CRS, CM, and DFG are partially supported by the National Science Foundation (grant nos: CMMI 1635430 and OISE-1243482, the WINDINSPIRE project). JM is supported by the European Research Council (ActiveWindFarms, grant no: 306471).

[1]Carl R. Shapiro, Charles Meneveau, and Dennice F. Gayme are with the Department of Mechanical Engineering, Johns Hopkins University, Baltimore, Maryland 21218, USA crshapiro@jhu.edu, meneveau@jhu.edu, dennice@jhu.edu

[2]Johan Meyers is with the Department of Mechanical Engineering, KU Leuven, 3001 Leuven, Belgium johan.meyers@kuleuven.be

For a single turbine, this power set point reduction (derating) can be accomplished by changing the tip speed ratio or blade pitch angle such that the power coefficient is less than optimal. A particularly effective approach [7] is to modify the generator torque control law such that the turbine operates at a higher-than-optimal tip speed ratio, thereby storing energy in the rotating rotor. Since a single wind turbine cannot provide power production greater than the maximum power point for an extended period, the derated generation setpoint is the maximum power point minus the regulation power.

While the single-turbine approach is effective when all wind turbines are operating in unwaked conditions, controlling the power output of an entire farm is complicated by wind turbine wakes and wake interactions. Control actions at an individual wind turbine modify the strength and characteristics of the wake behind the rotor, which in turn affects the subsequent power production of downstream turbines as the wake travels downwind. For example, suppose a turbine at the beginning of the farm pitches its blades from a feathered configuration toward the optimal pitch angle. The power generation at that turbine will increase, reducing the velocity in the turbine's wake. As a result, the generation of downstream turbines will decrease, but only after the wake has traveled to the downstream turbine. This complex and time-varying aerodynamic coupling of upstream turbine control actions and downstream turbine power generation is a particular challenge for secondary frequency regulation because the travel time of the wind from one turbine to the next and the time it takes the wind to travel the length of the farm is routinely the same or longer than the duration and frequency of typical regulation signals.

Several solutions have been proposed to address the technical challenges of controlling a wind farm's power output to track a reference signal. Attempts to use single-turbine approaches for multiple turbines in a farm resulted in significantly reduced power tracking performance [9]. To address these limitations, a proportional-integral controller was proposed that employs the same single-turbine control strategy but compensates for underperforming turbines by increasing the power production of other turbines operating below the maximum power point [4]. The resulting closed-loop wind farm provides good tracking performance in tests employing high-fidelity simulations as a wind farm model. However, the derate used in [4] was larger than the regulation power, sacrificing considerable revenue in the bulk power market. Finally, controllers based on static wake models that neglect wake travel dynamics are also unable to provide adequate power tracking performance [11].

In recent years, dynamic models have been proposed that

account for the movement of wakes through the wind farm as well as turbulent mixing of wakes with the surrounding air, either as extensions of the classic Jensen wake model [3], [12] or as an implementation of the two-dimensional Navier-Stokes equations [13]. A frequency regulation approach was proposed in [3], [11] that builds a controller around a dynamic wake model. It employs a model-based receding horizon controller, coupled with an ensemble Kalman filter for state and parameter estimation [14], to provide power tracking by modulating the thrust coefficients of each row of wind turbines. When this algorithm was tested using a high-fidelity simulation of an 84-turbine wind farm as a plant model, the controlled wind farm was shown to provide good power tracking while reducing the required derate.

In this work, we extend the model-based receding horizon controller proposed and validated in [3], [11] in three ways. First, we explicitly include actuation of blade pitch angle and generator torque, which were previously assumed to be parameterized by the thrust coefficient. Second, the wake model, which was previously one dimensional, is extended to two dimensions to allow for irregular wind farm configurations. Third, we include first-order drive train dynamics of the turbines, which enables the control of rotor speed and storage of kinetic energy in the rotating rotor. The rotor's ability to store kinetic energy has been shown to be useful in reducing turbulent power fluctuations in wind farms [15] and providing inertial frequency regulation [7]. The new generalized control framework is easier to implement in existing wind farms because it can be directly tied to existing wind turbine control loops and improves control authority by allowing direct control of each wind turbine. Numerical simulations illustrate the application of the approach to two wind farm configurations and demonstrate how the kinetic energy reserves are exploited to achieve the tracking objectives.

The remainder of this paper is organized as follows. Section II describes the improved wake model. The controller design is discussed in Section III. Simulations are discussed in Section IV. Conclusions are made in Section V.

II. WAKE AND TURBINE MODEL

The time-varying wake and turbine model described in this section is an extension of the model first proposed and validated in [3]. That model augmented the well-known Jensen model [16] to derive a one-dimensional dynamic model of the time evolution of the turbine wakes. It parameterized the turbine actions through the local thrust coefficient C'_T and assumed that each row of turbines operated collectively. The extended model proposed here explicitly includes blade pitch angle β and generator torque Q. It also incorporates the first-order drive train equations with inertia and rotational speed, and generalizes the superposition equations to accommodate irregular wind farm configurations.

Consider an N-turbine wind farm whose horizontal coordinates parallel and orthogonal to the prevailing wind U_∞ with density ρ are denoted as x and y, respectively. Here the wind direction is assumed to remain constant, although future work could extend the model to allow for changing orientations. The corresponding streamwise and lateral spatial extents of the farm are denoted as L_x and L_y, respectively. Each turbine has a rotor diameter of D and the n-th turbine is located at $(x, y) = (s_n^x, s_n^y)$. Each turbine rotor has a moment of inertia J and rotates at a speed ω_n. Turbine n is controlled via blade pitch angle β_n and generator torque Q_n.

The turbines are represented using an actuator disk model, where the control actions of the n-th turbine modify the thrust force and aerodynamic power via the thrust C_{Tn} and power C_{Pn} coefficients [17]. These coefficients are assumed to be functions of the pitch angle β_n and tip speed ratio $\lambda_n = \frac{\omega_n D}{2U_\infty}$ [17], [18]. We define the local [19], [20] thrust coefficient, power coefficient, and tip speed ratio as

$$C'_{Tn} = \frac{C_{Tn}}{(1-a_n)^2},\ C'_{Pn} = \frac{C_{Pn}}{(1-a_n)^3}, \text{and } \lambda'_n = \frac{\lambda_n}{1-a_n}, \quad (1)$$

where $a_n = 1 - \hat{u}/u_{\infty n}$ is the induction factor described by the ratio between the rotor-averaged velocity at the turbine $\hat{u}_n$ and the upstream velocity $u_{\infty n}$. Using the actuator disk model [19], [20], the induction factor is given by $4a_n(1 - a_n) = C_{Tn}$.

The thrust and power coefficient curves are modeled using blade element momentum theory [21]. Transformed curves based on the local rotor-averaged velocity $C'_T(\beta, \lambda')$ and $C'_P(\beta, \lambda')$ are obtained using interpolation. These relationships are implemented as lookup tables that are interpolated using monotone piecewise cubic interpolation [22].

As in the Jensen model [16], we assume that the diameter of the wake behind the n-th turbine grows linearly as it moves downstream at a rate k_n. This asymptotic linear growth is expressed by the normalized and smooth function

$$d_n(x) = 1 + k_n \ln\Big]1 + \exp\Big)\frac{x - s_n^x - D}{D/2}\Big[\Big(, \quad (2)$$

such that the wake diameter is $d_n(x)D$. Applying momentum and mass conservation across an infinitesimal control volume [3], the velocity deficit $\delta u_n(x, t)$ in the wake of the n-th turbine is governed by

$$\frac{\partial \delta u_n}{\partial t} + U_\infty \frac{\partial \delta u_n}{\partial x} = -w_n(x)\delta u_n(x, t) + f_n(x, t), \quad (3)$$

where the wake decay function

$$w_n(x) = 2\frac{U_\infty}{d_n(x)}\frac{d}{dx}d_n(x) \quad (4)$$

describes the expansion of the wake through the normalized wake diameter function $d_n(x)$, and the forcing function

$$f_n(x, t) = \frac{2U_\infty^2}{d_n^2(x)}\frac{C'_{Tn}(\beta(t), \lambda'(t))}{4 + C'_{Tn}(\beta(t), \lambda'(t))}G(x - s_n) \quad (5)$$

describes the effect of the turbine's thrust force on the wake velocity deficit itself. As described above, the local thrust coefficient is a function of the pitch angle and local tip speed ratio. The function

$$G(x - s_n) = \frac{1}{\Delta\sqrt{2\pi}}\exp\Big)-\frac{(x - s_n^2)^2}{2\Delta^2}\Big[\quad (6)$$

is a normalized Gaussian smoothing function with width $\Delta = D/2$ that spreads the velocity deficit forcing in the streamwise direction to ensure continuous velocity deficits.

After calculating the velocity deficits induced by each turbine, the wakes are combined to determine the velocity field using a modified version of the square-superposition approach in [16]. In particular, the velocity field is given by

$$u(x,y,t) = U_\infty - \Big)\sum_{n=1}^{N} \delta u_n^2(x,t) I_n(x,y) \Big(^{1/2}, \quad (7)$$

where $I_n(x,y)$ is the indicator function specifying the width of the wake defined by the normalized wake diameter

$$I_n(x,y) = H(d_n(x - s_n^x)D/2 - |y - s_n^y|), \quad (8)$$

and $H(x)$ is the Heaviside (unit step) function. The rotor-averaged velocity at each turbine is subsequently calculated by sampling this velocity field as

$$\hat{u}_n(t) = \int_0^{L_x}\int_0^{L_y} u(x,y,t) G(x - s_n^x)\tilde{H}(y - s_n^y)\, dy\, dx, \quad (9)$$

where $\tilde{H}(y) = D^{-1}H(D/2 - |y|)$ is a normalized top-hat function. The rotational speed $\omega_n(t)$ of the rotor is governed by first order drive-train dynamics [18]

$$\frac{d\omega_n}{dt} = \frac{1}{J}\Big)\frac{\hat{P}_n(t)}{\omega_n(t)} - Q_n(t)\Big[, \quad (10)$$

where $\hat{P}_n(t) = \frac{1}{8}\rho\pi D^2 C'_{Pn}\hat{u}_n^3(t)$ is the aerodynamic power. The power delivered by the generator to the power grid is

$$P_n(t) = Q_n(t)\omega_n(t). \quad (11)$$

We next present the controller design that uses the wake model described above to calculate control actuation.

III. CONTROLLER DESIGN

The control goal in secondary frequency regulation applications is tracking a reference signal $P_{\text{ref}}(t)$. Here we propose a method to achieve this regulation by controlling the power output of a wind farm, via actuating the blade pitch angles $\beta_n(t)$ and generator torques $Q_n(t)$ of each turbine. The power tracking goal is represented by the cost functional

$$\mathscr{J} = \int_{t_0}^{t_0+T}\Big)\sum_{n=1}^{N} Q_n(t)\omega_n(t) - P_{\text{ref}}(t)\Big[^2 dt, \quad (12)$$

where $Q_n(t)\omega_n(t)$ is the power generated by turbine n and t_0 is the current time. The control is then accomplished by solving the following minimization problem

$$\underset{\boldsymbol{\varphi}(t),\mathbf{q}(x,y,t)}{\text{minimize}} \quad \mathscr{J}(\mathbf{q}(x,y,t)) \quad (13)$$

$$\text{subject to} \quad \mathbf{W}(\mathbf{q}(x,y,t),\boldsymbol{\varphi}(t)) = \mathbf{0} \quad (14)$$

$$Q_n(t) = (1 - \alpha_n(t))\frac{\hat{P}_n(t)}{\omega_n(t)}. \quad (15)$$

The control inputs $\boldsymbol{\varphi}(t) = [\boldsymbol{\beta}_n(t), \boldsymbol{\alpha}_n(t)]$ include the blade pitch angle and an auxiliary control variable $\boldsymbol{\alpha}(t)$ that specifies the imbalance between the aerodynamic and generator torques; i.e. the torques $\hat{P}_n(t)/\omega_n(t) - Q_n(t) = \alpha_n(t)\hat{P}_n(t)/\omega_n(t)$ are balanced when $\alpha = 0$. This auxiliary control variable increases the computational efficiency of the minimization problem. The states of the wind farm model $\mathbf{q}(x,y,t) = [\boldsymbol{\delta}\mathbf{u}(x,t), u(x,y,t), \hat{\mathbf{u}}(t), \boldsymbol{\omega}(t)]$ are respectively the wake velocity deficits, superposed velocity field, rotor-averaged velocities, and rotor speeds. The dynamics of the states are governed by the wind farm model $\mathbf{W}(\mathbf{q}(x,y,t),\boldsymbol{\varphi}(t)) = \mathbf{0}$ in (2)–(11). This wind farm model and generator torque equation (15) are represented in discrete-time state space form as

$$\mathbf{q}_{k+1} = \mathbf{f}(\mathbf{q_k}, \boldsymbol{\varphi}_k) \quad (16)$$

$$\mathbf{z}_k = \mathbf{h}(\mathbf{q_k}, \boldsymbol{\varphi}_k). \quad (17)$$

The nonlinear functions $\mathbf{f}(\mathbf{q_k}, \boldsymbol{\varphi}_k)$ are first-order temporal and spatial discretizations of (2)–(10) and (15). The outputs are the power output of each turbine $\mathbf{z}(t) = \mathbf{P}(t)$, and the nonlinear output equation $\mathbf{h}(\mathbf{q_k}, \boldsymbol{\varphi}_k)$ corresponds to (11).

The controller calculates control trajectories for pitch angle and generator torque by solving a reformulation of (13)–(15) using a receding horizon approach, where T is the length of the time horizon considered. The horizon length is selected to include a significant fraction of the advection time through the farm; i.e. $T \sim L_x/U_\infty$. Instead of directly solving the PDE-constrained optimization problem (13)–(15), we solve the related unconstrained minimization of the reduced cost functional $\tilde{\mathscr{J}}(\boldsymbol{\varphi}) = \mathscr{J}(\boldsymbol{\varphi}, \mathbf{q}(\boldsymbol{\varphi}))$, where $\mathbf{q}(\boldsymbol{\varphi})$ denotes the solution of (14). The reduced cost functional is evaluated by integrating the wind farm model forward in time, and its gradient is evaluated using adjoint equations derived analytically using the formal Lagrangian approach [24]. The minimization is performed using a limited-memory bound-constrained quasi-Newton method [25]. The optimization method is described in detail in [3].

IV. RESULTS

The controller design is validated using a model of a 16-turbine wind farm based on (2)–(11). Each turbine is an NREL 5MW offshore reference turbine [23] with a rotor diameter of $D = 126$ m. Two layouts (regular and irregular), shown in Figure 1, are used with an inflow velocity of $U_\infty = 9$ m/s and a constant wake expansion coefficient of $k_n = 0.05$. This coefficient value is typical of offshore wind farms [26], and the inlet velocity chosen assumes each turbine is operating in region 2. The first layout is composed of four aligned rows with streamwise and spanwise spacings of $7D$ and $5D$, respectively. The second irregular layout is formed by randomly offsetting turbines from the first layout. The full block diagram of the controlled wind farm considered is shown in Figure 2. The same wake and turbine model discussed in Section II (2)–(11) is used both in the controller and as the wind farm plant model.

All controlled cases are compared to the behavior of a wind farm operating under the traditional maximum power point control paradigm; i.e. each turbine operates at its maximum power point in region 2. In this regime, the blade

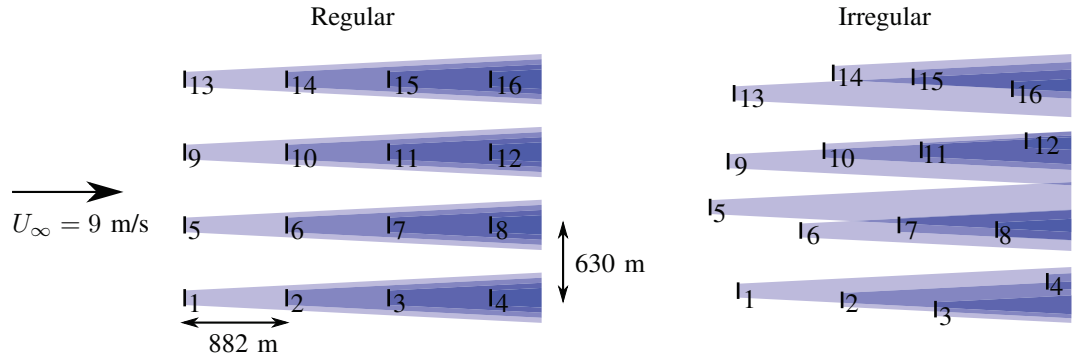

Fig. 1. Two wind farm layouts considered, each with sixteen NREL 5MW turbines [23]. The regular wind farm (left) has four aligned rows of turbines, with streamwise and spanwise spacings shown. The irregular layout (right) has been randomly offset from the regular layout. The inflow velocity, which is the same for each layout, is shown to the left and the extent of the wakes with $k = 0.05$ is shown in blue.

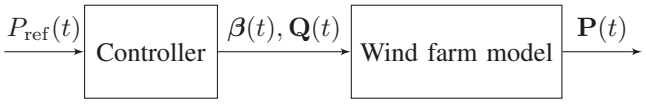

Fig. 2. Controlled wind farm system block diagram showing the model-based receding horizon controller and model wind farm. $P_{\text{ref}}(t)$ is the power reference signal, $\boldsymbol{\beta}(t)$ is the vector of pitch angles, $\mathbf{Q}(t)$ is the vector of generator torque, and $\mathbf{P}(t)$ is the vector of measured power generation.

pitch angle is kept fixed at the optimal value $\beta = \beta_*$ and the generator torque $Q = K\omega^2$ has a gain $K = \frac{1}{2}\rho\pi \left(\frac{D}{2}\right)^5 \frac{C_{P*}}{\lambda_*^3}$ [18] that drives the tip speed ratio to the optimal power coefficient $C_{P*} = C_P(\lambda_*, \beta_*)$. Since each turbine operates to maximize its own power production, rather than farm-level power, this operating condition is sometimes referred to as "greedy" control [27].

The reference signal is composed of a fixed power generation level P_0, which would typically be sold in the bulk power market, and a power regulation reserve ΔP that can be provided in the regulation market. The resulting signal is

$$P_{\text{ref}}(t) = P_0 + \Delta P\, r(t), \tag{18}$$

where the regulation signal $-1 \le r(t) \le 1$ is used by the grid operator to modulate the regulation power delivered by the farm. We select a bulk power supply of $P_0 = 0.85P_*$, where P_* is the "greedy" pre-control generation, and a regulation supply of $\Delta P = 0.3P_*$. This corresponds to a derate (power setpoint reduction) of only 50% of ΔP. We use a synthetic regulation signal $r(t)$, shown in red in Figure 3, that declines to $r(t) = 0$ for the first 10 minutes before requesting an up-regulation of $r(t) = 1$ between 10:00 min and 15:00 min. The up-regulation ramp is $\Delta P = 0.3P_*$ and lasts for 5 minutes, which is approximately the travel time of the wind through the entire farm.

In both the regular and irregular layout, the controlled power output closely follows the power reference signal, as shown in Figure 3. The root mean square error

$$RMSE = \left(\frac{1}{T}\int_0^T \left[\sum_{n=1}^{N} Q_n(t)\omega_n(t) - P_{\text{ref}}(t)\right]^2 dt\right)^{\frac{1}{2}} \tag{19}$$

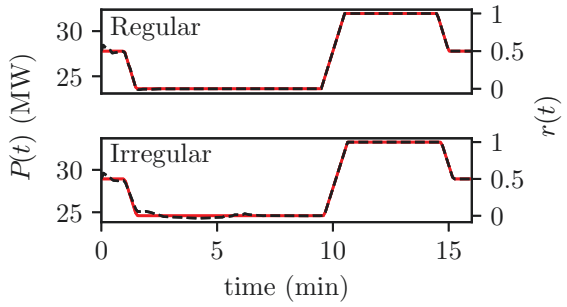

Fig. 3. Total wind farm power output of both regular and regular layouts $P(t) = \sum_{n=1}^{N} P_n(t)$ (– – –) compared to reference signal $P_{\text{ref}}(t)$ (——). The regulation signal $r(t)$ is also shown on the right side ordinate.

is 0.24% and 0.56% of P_* for the regular and irregular configurations, respectively. This tracking performance is achieved with a signal that exceeds the "greedy" control power for a short period of time. This short-term over production is achieved by storing energy in the flow field and adjusting the rotational speed to hold kinetic energy in the rotors of the turbines, as described in more detail below.

In the regularly arranged layout, the wakes do not expand enough to create spanwise interactions. As a result, the controller selects pitch and torque signals that are the same for all turbines in a particular row; i.e. the signals for turbines 1, 5, 9, and 13 are all the same. In a real wind farm, turbulent fluctuations in the wind field would break the equivalence of the control actions within a row. The power generation response of the controller for the turbines in the first column (turbines 1–4) is shown in Figure 6. The controller reduces the power generation of the first and last rows just preceding the up-regulation period, while keeping the generation of the second and third rows of turbines close to the pre-control power. The resulting generation during the up-regulation period is higher than the pre-control period for all downstream turbines, but this effect could not be sustained indefinitely. Since the first row of turbines cannot sustain generation higher than the optimal power point for five minutes, the first turbine produces near its pre-control output during the up-regulation period.

Fig. 4. Response of regular layout turbines 1 (——), 2 (– – –), 3 (- - -), and 4 (— -) showing the pitch angle β, the auxiliary control variable α, generator torque Q, rotor speed ω, rotor-averaged velocity $\hat{u}$, local tip speed ratio λ', local thrust coefficient C'_T, local power coefficient C'_P, and the generated power P. The up-regulation period $r(t) > 0.5$ is shaded gray between minutes 10 and 15.

Fig. 5. Response of all turbines in the irregular layout. The panels show the pitch angle β, generator torque Q, and generated power P. The up-regulation period $r(t) > 0.5$ is shaded gray between minutes 10 and 15. Colors denote turbines 1–4 (——), 5–8 (——), 9–12 (——), 13–16 (——).

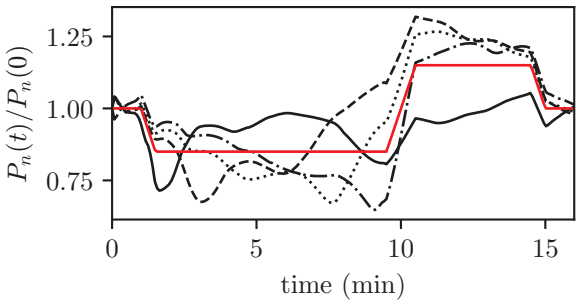

Fig. 6. Power generation of regular layout turbines 1 (——), 2 (– – –), 3 (- - -), and 4 (— -) normalized by their "greedy" pre-control power generation compared to $P_{\text{ref}}(t)/P_*$ (——). Only one column is shown because all turbines in a row of the regular layout have the same control. Increased generation of turbines 2–4 for the 5-minute up-regulation period is enabled by storing energy in the flow field and rotation of the rotors.

The pitch angle β, auxiliary control variable α, generator torque Q, rotor speed ω, rotor-averaged velocity $\hat{u}$, local tip speed ratio λ', local thrust coefficient C'_T, local power coefficient C'_P, and the generated power P trajectories for the first column of the regular layout are shown in Figure 4. The controller sequentially decreases the thrust and power coefficients of the upstream turbines, turbine 1 around $t =$ 5:30 min, turbine 2 around $t =$ 7:00 min, and turbine 3 around $t =$ 8:30 min. These decreases in thrust coefficient reduce the magnitude of the wakes between the turbines, thus allowing higher velocity air to reach downstream turbines. The time of the decreases is closely tied to the advection time between turbines ($\approx$ 90 s), allowing the velocity at each turbine to peak around 10:00 min.

The controller simultaneously uses pitch and generator torque to reduce the power production of the upstream turbines prior to the up-regulation period. All turbines pitch to feather between 8:00 min and 10:00 min, dropping the power and thrust coefficients. Furthermore, the generator torques are increased to slow down the rotor speed and reduce the tip speed ratio. On the other hand, the last turbine keeps its rotor speed slightly higher than the optimal tip speed ratio. This action stores kinetic energy that can later be extracted during the up-regulation period at 10:00 min.

The input and output trajectories for each turbine of the irregular layout are shown in Figure 5. In this layout, each turbine has a different wake state and therefore the output power and control signals follow unique trajectories. However, the general trends of the regular configuration are also seen in these results. The thrust coefficients of upstream turbines decline prior to the up-regulation period via pitch-to-feather and increased generator torque actuation. Downstream turbines show a slight over-speeding of their rotors to store energy for the up-regulation period.

V. CONCLUSIONS

We present a generalized dynamic wake model that allows for irregular wind farm configurations, explicitly includes actuation of blade pitch angle and generator torque, and incorporates first-order drive train dynamics. These improvements are a significant step towards implementation of previously proposed model-based receding horizon control using existing wind turbine control loops. Control authority is improved by separately controlling each turbine and accounting for kinetic energy stored in the rotors.

Testing of the controller using wind farm plants consisting of the wake and turbine model and a synthetic power reference signal demonstrate the potential of this control design. Accounting for wake interactions and exploiting the storage of kinetic energy in the rotor, the controller is able to provide regulation power with derates less than the amount of regulation provided; i.e. $P_0 < P_* - \Delta P$. Further work includes adding a state and parameter estimation model [14] as well as testing the closed-loop controller in high-fidelity wind farm simulations [11] and operating wind farms. More work is also needed to directly compare our model-based approach to other potential controllers built around alternative models or proposed proportional-integral methods [4]. Finally, other ongoing work includes extending the model and control approach to yawing turbines and changing wind directions.

APPENDIX

The adjoint equations and the gradient of the reduced cost functional are derived using the formal Lagrangian approach [24]. We define the Lagrangian of the PDE-constrained problem by adding the inner product $\langle\cdot,\cdot\rangle$ of the constraining set of equations (14)–(15), denoted as $\mathbf{B}(\mathbf{q},\boldsymbol{\varphi})$, and a suitable set of Lagrange multipliers $\mathbf{q}^* = [\boldsymbol{\delta}\mathbf{u}^*(x,t), u^*(x,y,t), \hat{\mathbf{u}}^*(t), \boldsymbol{\omega}^*(t)]$ to the cost functional (13) $\mathscr{L}(\boldsymbol{\varphi},\mathbf{q},\mathbf{q}^*) = \mathscr{J}(\boldsymbol{\varphi},\mathbf{q}) + \langle\mathbf{B}(\mathbf{q},\boldsymbol{\varphi}),\mathbf{q}^*\rangle$. The adjoint equations $\mathbf{B}^*(\boldsymbol{\varphi},\mathbf{q},\mathbf{q}^*)$ are found by representing the Gateaux derivative of the Lagrangian with respect to the state variables in its Riesz representation form $\mathscr{L}_{\mathbf{q}}(\boldsymbol{\Delta}\mathbf{q}) = \langle\mathbf{B}^*(\boldsymbol{\varphi},\mathbf{q},\mathbf{q}^*),\boldsymbol{\Delta}\mathbf{q}\rangle$. The adjoint equations

$$-\frac{\partial\delta u_n^*}{\delta t} - U_\infty\frac{\partial\delta u_n^*}{\partial x} = -w_n(x)\delta u_n^*(x,t) + f_n^*(x,t) \quad (20)$$

$$u^*(x,y,t) = \int_{n=1}^{N} G(x-s_n^x)\frac{I_n(x,y)}{Dd_n(x)}\hat{u}_n^*(t) \quad (21)$$

$$\begin{aligned}\hat{u}_n^*(t) =& U_{\mathscr{J}n}(t) + U_{\omega n}(t)\omega_n^*(t)\\ &+ U_{\delta un}(t)\int_0^{L_x} f_n(x,t)\delta u_n^*(x,t)\,dx\end{aligned} \quad (22)$$

$$\begin{aligned}-\frac{d\omega_n^*}{dt} =& W_{\mathscr{J}n}(t) + W_{\omega n}(t)\omega_n^*(t)\\ &+ W_{\delta un}(t)\int_0^{L_x} f_n(x,t)\delta u_n^*(x,t)\,dx.\end{aligned} \quad (23)$$

are integrated backward in time with final time boundary conditions. The forcing for the adjoint velocity deficits and the terms on the right hand sides of (22) and (23) are

$$\begin{aligned}f_n^*(x,t) = -\delta u_n(x,t)&\int_0^{L_y} I_n(x,y)u^*(x,y,t)\\ &\Bigg)\int_{m=1}^{N}\delta u_m^2(x,t)I_m(x,y)\Bigg[^{-1/2}\,dy\end{aligned}$$

$$U_{\mathscr{J}n}(t) = -2\Bigg)\int_{m=1}^{N}[1-\alpha_m(t)]\,\hat{P}_m(t) - P_{\text{ref}}(t)\Bigg[$$
$$[1-\alpha_n(t)]\,\hat{P}_n(t)\Bigg]\frac{3}{\hat{u}_n(t)} - \frac{\omega_n(t)R}{C'_{Pn}(t)\hat{u}_n^2(t)}\frac{\partial C'_{Pn}}{\partial\lambda'_n}\Bigg($$
$$U_{\omega n}(t) = \frac{\alpha_n(t)}{J}\hat{P}_n(t)\Bigg]\frac{3}{\omega_n(t)\hat{u}_n(t)} - \frac{R}{C'_{Pn}(t)\hat{u}_n^2(t)}\frac{\partial C'_{Pn}}{\partial\lambda'_n}\Bigg($$
$$U_{\delta un}(t) = -\frac{4}{C'_{Tn}(t)}\frac{1}{4+C'_{Tn}(t)}\frac{\partial C'_{Tn}}{\partial\lambda'_n}\frac{\omega_n(t)R}{\hat{u}_n^2(t)}$$
$$W_{\mathscr{J}n}(t) = -2\Bigg)\int_{m=1}^{N}[1-\alpha_m(t)]\,\hat{P}_m(t) - P_{\text{ref}}(t)\Bigg[$$
$$[1-\alpha_n(t)]\,\hat{P}_n(t)\frac{1}{C'_{Pn}(t)}\frac{\partial C'_{Pn}}{\partial\lambda'_n}\frac{R}{\hat{u}_n(t)}$$
$$W_{\omega n}(t) = \frac{\alpha_n(t)}{J}\Bigg]\frac{\hat{P}_n(t)}{\omega_n(t)}\frac{1}{C_{Pn'}(t)}\frac{\partial C'_{Pn}}{\partial\lambda'_n}\frac{R}{\hat{u}_n(t)} - \frac{\hat{P}_n(t)}{\omega_n^2(t)}\Bigg($$
$$W_{\delta un}(t) = \frac{4}{C'_{Tn}(t)}\frac{1}{4+C'_{Tn}(t)}\frac{\partial C'_{Tn}}{\partial\lambda'_n}\frac{R}{\hat{u}_n(t)}.$$

The gradient of the reduced cost functional $\partial\tilde{\mathscr{J}}/\partial\boldsymbol{\varphi}$ is found by representing the Gateaux derivative of the Lagrangian with respect to the control variables in its Riesz representation form $\mathscr{L}_{\boldsymbol{\varphi}}(\boldsymbol{\Delta\varphi}) = \left\langle\partial\tilde{\mathscr{J}}/\partial\boldsymbol{\varphi}, \boldsymbol{\Delta\varphi}\right\rangle_{\Sigma}$

$$\frac{\partial\tilde{\mathscr{J}}}{\partial\alpha_n} = \Bigg]-2\Bigg)\int_{m=1}^{N}[1-\alpha_m(t)]\,\hat{P}_m(t) - P_{\text{ref}}(t)\Bigg[\quad (24)$$
$$-\frac{\omega_n^*(t)}{J}\hat{P}_n(t)\frac{1}{\omega_n(t)}\Bigg(\hat{P}_n(t)$$
$$\frac{\partial\tilde{\mathscr{J}}}{\partial\beta_n} = B_{\mathscr{J}n}(t) + B_{\omega n}(t)\omega_n^*(t) \quad (25)$$
$$+ B_{\delta un}(t)\int_0^{L_x} f_n(x,t)\delta u_n^*(x,t)\,dx,$$

where the coefficients are

$$B_{\mathscr{J}n}(t) = 2\Bigg)\int_{m=1}^{N}[1-\alpha_m(t)]\,\hat{P}_m(t) - P_{\text{ref}}(t)\Bigg[$$
$$[1-\alpha_n(t)]\,\hat{P}_n(t)\frac{1}{C'_{Pn}(t)}\frac{\partial C'_{Pn}}{\partial\beta_n}$$
$$B_{\omega n}(t) = -\frac{\alpha_n(t)}{J}\hat{P}_n(t)\frac{1}{\omega_n(t)}\frac{1}{C'_{Pn}(t)}\frac{\partial C'_{Pn}}{\partial\beta_n}$$
$$B_{\delta un}(t) = -\frac{4}{C'_{Tn}(t)}\frac{1}{4+C'_{Tn}(t)}\frac{\partial C'_{Tn}}{\partial\beta_n}.$$

REFERENCES

[1] F. Díaz-González, M. Hau, A. Sumper, and O. Gomis-Bellmunt, "Participation of wind power plants in system frequency control: Review of grid code requirements and control methods," *Renew. Sust. Energy Rev.*, vol. 34, pp. 551–564, 2014.

[2] J. Aho, A. Buckspan, J. Laks, P. Fleming, Y. Jeong, F. Dunne, M. Churchfield, L. Pao, and K. Johnson, "A tutorial of wind turbine control for supporting grid frequency through active power control," in *American Control Conf.*, Montreal, Canada, 2012, pp. 3120–3131.

[3] C. R. Shapiro, P. Bauweraerts, J. Meyers, C. Meneveau, and D. F. Gayme, "Model-based receding horizon control of wind farms for secondary frequency regulation," *Wind Energy*, vol. 20, no. 7, pp. 1261–1275, 2017.

[4] J.-W. van Wingerden, L. Pao, J. Aho, and P. Fleming, "Active power control of waked wind farms," in *Int. Federation Automat. Control World Congr.*, Toulouse, France, 2017.

[5] S. Rose and J. Apt, "The cost of curtailing wind turbines for secondary frequency regulation capacity," *Energy Systems*, vol. 5, no. 3, pp. 407–422, 2014.

[6] B. Kirby, M. Milligan, and E. Ela, "Providing minute-to-minute regulation from wind plants," in *9th Ann. Large-Scale Integration of Wind Power into Power Systems and Transmission Networks for Offshore Wind Power Plants*, Quebec City, Canada, 2010.

[7] J. Aho, L. Pao, and P. Fleming, "An active power control system for wind turbines capable of primary and secondary frequency control for supporting grid reliability," in *51st AIAA Aerospace Sciences Meeting*, Grapevine, TX, 2013, p. 456.

[8] Y. Jeong, K. Johnson, and P. Fleming, "Comparison and testing of power reserve control strategies for grid-connected wind turbines," *Wind Energy*, vol. 17, no. 3, pp. 343–358, 2014.

[9] P. Fleming, J. Aho, P. Gebraad, L. Pao, and Y. Zhang, "Computational fluid dynamics simulation study of active power control in wind plants," in *American Control Conf.*, Boston, MA, 2016, pp. 1413–1420.

[10] S. Boersma, B. M. Doekemeijer, P. M. O. Gebraad, P. A. Fleming, J. Annoni, A. K. Scholbrock, J. A. Frederik, and J.-W. van Wingerden., "A tutorial on control-oriented modeling and control of wind farms," in *American Control Conf.*, Seattle, WA, 2017, pp. 1–18.

[11] C. R. Shapiro, J. Meyers, C. Meneveau, and D. F. Gayme, "Wind farms providing secondary frequency regulation: Evaluating the performance of model-based receding horizon control," *Wind Energy Sci.*, vol. 3, pp. 11–24, 2018.

[12] P. M. O. Gebraad and J. W. van Wingerden, "A control-oriented dynamic model for wakes in wind plants," *J. Physics: Conf. Series*, vol. 524, p. 012186 2014.

[13] B. M. Doekemeijer, S. Boersma, L. Y. Pao, and J. W. van Wingerden, "Ensemble kalman filtering for wind field estimation in wind farms," in *American Control Conf.*, Seattle, WA, May 2017, pp. 19–24.

[14] C. R. Shapiro, J. Meyers, C. Meneveau, and D. F. Gayme, "Dynamic wake modeling and state estimation for improved model-based receding horizon control of wind farms," in *American Control Conf.*, Seattle, WA, 2017, pp. 709–716.

[15] S. De Rijcke, J. Driesen, and J. Meyers, "Power smoothing in large wind farms using optimal control of rotating kinetic energy reserves," *Wind Energy*, vol. 18, no. 10, pp. 1777–1791, 2015.

[16] I. Katic, J. Højstrup, and N. O. Jensen, "A simple model for cluster efficiency," in *EWEA Conf.*, Rome, Italy, 1986, pp. 407–410.

[17] T. Burton, N. Jenkins, D. Sharpe, and E. Bossanyi, *Wind Energy Handbook*. John Wiley & Sons, 2011.

[18] L. Y. Pao and K. E. Johnson, "Control of wind turbines," *IEEE Control Syst. Mag.*, vol. 31, no. 2, pp. 44–62, 2011.

[19] J. Meyers and C. Meneveau, "Large eddy simulations of large wind-turbine arrays in the atmospheric boundary layer," in *48th AIAA Aerospace Sci. Meeting*, 2010, p. 827.

[20] M. Calaf, C. Meneveau, and J. Meyers, "Large eddy simulation study of fully developed wind-turbine array boundary layers," *Phys. Fluids*, vol. 22, no. 1, p. 015110, 2010.

[21] M. O. Hansen, *Aerodynamics of wind turbines*. Earthscan, 2008.

[22] F. Fritsch and R. Carlson, "Monotone piecewise cubic interpolation," *SIAM J. Numerical Anal.*, vol. 17, no. 2, pp. 238–246, 1980.

[23] J. Jonkman, S. Butterfield, W. Musial, and G. Scott, "Definition of a 5-mw reference wind turbine for offshore system development," NREL, Tech. Rep. NREL/TP-500-38060, 2009.

[24] A. Borzì and V. Schulz, *Computational optimization of systems governed by partial differential equations*. SIAM, 2011.

[25] C. Zhu, R. H. Byrd, P. Lu, and J. Nocedal, "Algorithm 778: L-BFGS-B: Fortran subroutines for large-scale bound-constrained optimization," *ACM Trans. Math. Software*, vol. 23, no. 4, pp. 550–560, 1997.

[26] R. J. Barthelmie and L. E. Jensen, "Evaluation of wind farm efficiency and wind turbine wakes at the Nysted offshore wind farm," *Wind Energy*, vol. 13, no. 6, pp. 573–586, 2010.

[27] W. Munters and J. Meyers, "An optimal control framework for dynamic induction control of wind farms and their interaction with the atmospheric boundary layer," *Philosoph. Trans. Roy. Soc. A*, vol. 375, p. 20160100, 2017.